

MODELLING OF HEAT TRANSFER IN NON-ADIABATIC MONOLITH REACTORS AND EXPERIMENTAL COMPARISONS OF METAL MONOLITHS WITH PACKED BEDS

M. FLYTZANI-STEPHANOPOULOS,[†] G. E. VOECKS and T. CHARNG
Jet Propulsion Laboratory, California Institute of Technology, Pasadena, CA 91109, U.S.A.

(Received 15 August 1984)

Abstract—Heat transfer in metal honeycomb monoliths, under non-adiabatic conditions, is considered in this work. Using a simple geometric simulation of the monolithic structure, steady-state heat balances are written separately for the solid and gas phases of the simulated monolith. In the absence of chemical reaction the model is solved analytically to give solid and gas temperature profiles radially and axially within the monolith. An experimental system is used to compare heat transfer in a honeycomb metal monolith to the model predictions. Also, heat transfer in a packed bed of ceramic pellets is studied experimentally and compared to the metal monolith under similar, non-adiabatic conditions. Results point out the different heat-transfer merits of each of these two bed configurations.

INTRODUCTION

In recent years, monolithic catalyst supports have been considered as an alternative geometry to conventional packed beds of pellets. Typical ceramic or metallic monoliths consist of a honeycomb array of parallel channels of different shapes with catalytic material deposited on the channel walls. Notable advantages of monolithic structures include: (a) higher surface-to-volume ratio; (b) structural durability; (c) very low pressure drop (one to two orders of magnitude lower than in packed beds) and (d) uniform flow distribution within the honeycomb matrix. Another attractive feature of monoliths is the accessibility of catalyst (on the monolithic walls) which results in faster reaction kinetics than when limited by pore diffusion (pellet catalysts). Therefore, the monolith system provides for more flexible reactor design.

In designing more energy efficient catalyst systems, heat transfer to and from the catalyst must be optimized. Proper transfer of heat in chemical reaction systems is necessary for controlling side reactions, maintaining catalyst activity and conserving energy. Energy conservation can be better realized in systems where heat transfer by conduction and convection is more important than radiant heat transfer. Packed beds of ceramic pellets conduct heat poorly and large temperature gradients often exist radially and axially within the bed. Radial heat transfer is particularly important in endothermic reaction systems such as steam reforming of hydrocarbons where external heating through the reactor walls must be provided. The main medium for radial heat transfer in a pellet bed is the radially flowing gas. A typical honeycomb

monolith, on the other hand, does not allow for radial gas flow since it is a parallel channel system. However, its cellular structure provides a continuum for radial heat conduction as compared to the edge and point contact of pellets in a packed bed reactor. A ceramic monolith support, because of its low thermal conductivity and the lack of radial gas flow (and heat transfer), tends to function in an adiabatic mode. A metallic monolith provides for improved radial heat transfer because of its higher thermal conductivity and direct contact of its external walls with the metallic reactor shell. A metal monolith, clearly a non-adiabatic system, can function in a quasi-isothermal mode. Theoretical studies of monoliths (Hegedus, 1975; Votruba *et al.*, 1975; Heck *et al.*, 1976; Aris, 1977) have focused on ceramic honeycomb monoliths (for automobile exhaust cleanup, catalytic combustion, *etc.*) operating under nearly adiabatic conditions. Temperature and gas concentration profiles in all channels of the adiabatic monolith are nearly the same so that analysis and modelling of one channel suffice.

In a non-adiabatic honeycomb monolith different conditions prevail in each channel and interactions among different channels through conduction dictate the simultaneous consideration of the large number of monolith channels. Such is the case with metal monolith supports which have been considered for steam reforming of hydrocarbons (Flytzani-Stephanopoulos and Voecks, 1981). In that work both metal monoliths and packed beds were used in steam reforming of *n*-hexane, and distinct advantages of monoliths in both heat transfer and activity were demonstrated. As shown in Fig. 1, the temperature gradient between reactor wall and bed centreline in the initial third of the catalyst bed length was found to be over 30% lower with a metal monolith than with a conventional pellet bed. In addition, the conversion (based on the total hydrocarbons present) was more than five times higher in the monolith than the pellet bed. These findings

[†]Author to whom correspondence should be addressed. Present address: Department of Chemical Engineering, Room 66-501, Massachusetts Institute of Technology, Cambridge, MA 02139, U.S.A.

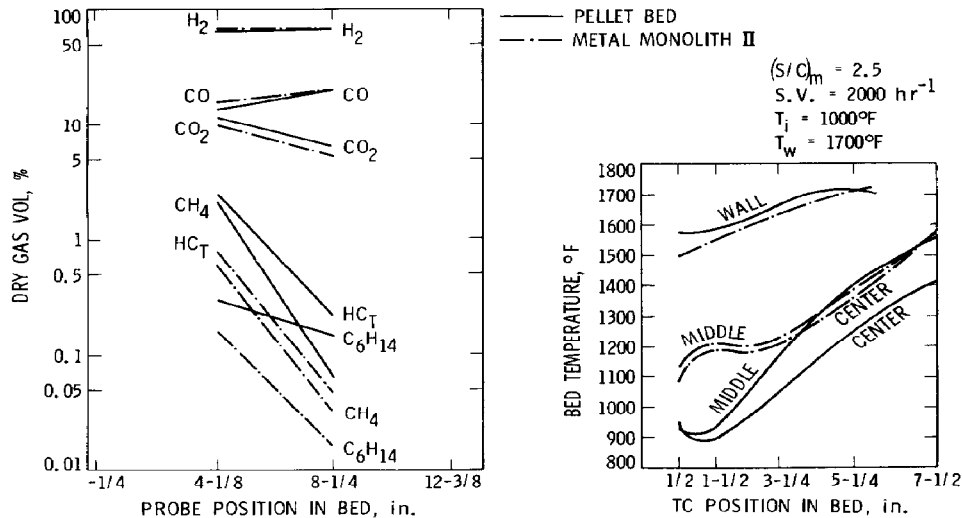


Fig. 1. Steam reforming of *n*-hexane. Axial bed temperature and composition profiles are for a metal monolith with 250 cells/in.², consisting of Kanthal support/ γ -Al₂O₃ washcoat/NiO catalyst, and a packed bed of Girdler G-90 C pellets (1/4" \times 1/4") of alumina impregnated with nickel.

indicated that the thermal efficiency of a steam reformer may be improved by selecting a different catalyst/support geometry. In order to delineate the heat transfer characteristics pertaining to each catalyst bed configuration (pellet or monolith), further work was focused on comparative heat transfer studies of metal monoliths and pellet beds under similar, non-adiabatic conditions. To simplify the comparison, heat transfer in the absence of chemical reaction was considered first. In this paper, a simple mathematical model of heat transfer in a metal monolith is developed and compared to experimental data. Comparisons of heat transfer in metal monoliths and packed beds are also made under similar experimental conditions.

MODEL DEVELOPMENT

A honeycomb monolith may be viewed as a series of concentric cylindrical rings of small width, l , each consisting of a number of small channels (cells) as shown in Fig. 2(a). Thin solid slabs of width l , thickness $2w$ and height H connect these rings to each other at the walls, which have zero thickness [Figure 2(b)]. Thus, the solid mass of the monolith is assumed to be distributed only along the radial direction. This assumption reduces the transverse heat conduction in the solid to one-dimensional (radial) only. At any monolith cross-section along the axial direction z , each of these visualized concentric wall-lines has uniform temperature (θ -symmetry). For very small channels, curvature effects can be neglected and the cylindrical coordinates may be replaced by rectangular ones.

A model of heat transfer within the monolithic structure of Fig. 2, in the absence of chemical reaction, is constructed by considering the following transport

mechanisms:

- convective heat transfer in the monolith channels,
- interphase heat transfer between the flowing gas and solid structure,
- radial heat conduction in the solid.

In this model, it is assumed that axial heat conduction in the solid is negligible and that no heat loss takes place from the monolith. In each monolith channel, uniform properties (ρ , C_p , μ , k_g , h) are assumed for the flowing gas. Also, an average value, $\langle v \rangle$, is used for the linear gas velocity in each channel. No radial heat conduction in the gas phase is considered. This means that the gas-phase temperature, T_g , is uniform across a channel cross-section. Due to θ -symmetry, all channels of the same ring will have identical gas temperatures. From each ring to the next, however, T_g is different because of heat conduction through the solid. The heat balance equations for the solid and gas phases of the monolith are derived based on the above assumptions.

(a) Steady-state heat balance for the solid phase

Consider n rings, each of length l along the x direction as shown in Fig. 3. At the monolith centre, $x = 0$, while at the external monolith wall, $x = nl = R$. The heat balance for the solid is made on one slab (fin) of the i th monolith ring, since all cells within each ring are equivalent. Heat is transferred by conduction through the solid slab of cross-section $2wH$. Continuity of heat fluxes is assumed at the ends of each slab (of length l) relating each ring to the next. Hence, the solid phase of the monolith is represented as a series of cooling fins (Bird *et al.*, 1960). The one-dimensional differential heat balance equation for the

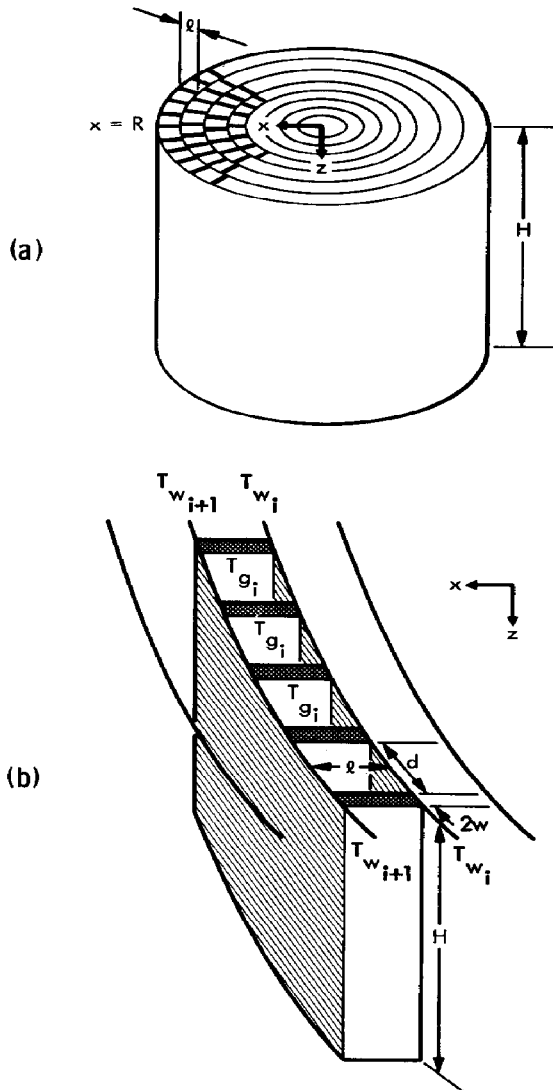


Fig. 2. (a) Schematic of a honeycomb monolith depicting the concentric rings used in the simulation. (b) Detail of (a) showing cells within the i th monolith ring.

solid temperature in the i th ring, T_{s_i} , at steady-state is:

$$\frac{d^2 T_{s_i}}{d\xi^2} = N^2 (T_{s_i} - T_{g_i}) \quad (1)$$

with

$$N^2 = \frac{hl^2}{k_s w} \text{ and } \xi = \frac{x - (i-1)l}{l}, 0 \leq \xi \leq 1 \quad (2)$$

where h is the heat transfer coefficient and k_s the solid thermal conductivity. At the L.H.S. boundary ($\xi = 1$) of the i th ring, $T_{s_i} = T_{w_i}$, $dT_{s_i}/d\xi = \beta_i$, where T_w denotes a wall temperature and β_i is the temperature gradient at the wall. Note that because of continuity:

$$T_{s_i}|_{\xi=0} = T_{s_{i-1}}|_{\xi=1} = T_{w_{i-1}} \quad (3)$$

and

$$\frac{dT_{s_i}}{d\xi}|_{\xi=0} = \frac{dT_{s_{i-1}}}{d\xi}|_{\xi=1} = \beta_{i-1}.$$

Equation (1) with boundary conditions (3) can be solved analytically. Its solution is:

$$T_{s_i} = T_{g_i} + (T_{w_i} - T_{g_i}) \cosh N(1 - \xi) - \frac{\beta_i}{N} \sinh N(1 - \xi). \quad (4)$$

Equation (4) gives the solid temperature for each monolith ring i as a function of ξ and T_{g_i} (uniform with respect to ξ). In order to find an expression for the wall temperature at any point of the monolith structure, eq. (4) will be used along with overall boundary conditions applied at the monolith centreline and external wall:

$$\frac{dT_{s_i}}{d\xi}|_{\xi=0} = \beta_0 = 0; \quad x = 0, z \geq 0 \quad (5)$$

$$T_{w_n} = T_w; \quad x = nl, z \geq 0 \quad (6)$$

where eq. (5) is the "no heat-sink" boundary condition, and eq. (6) prescribes a constant external wall temperature, uniform with z (alternatively, a constant heat flux could be prescribed on the external wall). The general formula derived for the wall temperature T_w , (at $x = il$)

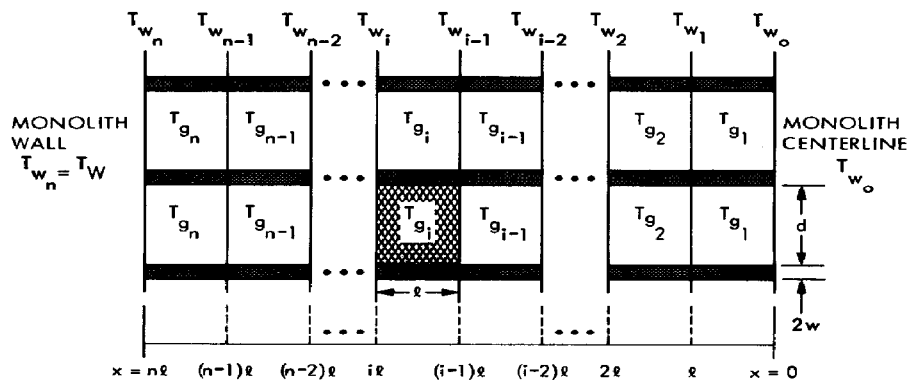


Fig. 3. Mathematical representation of the monolith solid phase on which heat balance is made. Cell positions and assigned temperatures are indicated.

is then:

$$T_{w_i} = T_{w_0} \cosh iN + \sum_{j=1}^i T_{g_j} [\cosh (i-j)N - \cosh (i-j+1)N]. \quad (7)$$

The temperature at the monolith centreline, T_{w_0} , is calculated by using eq. (7) at $i = n$, where $T_{w_n} = T_w$ (known).

(b) *Steady-state heat balance for the gas phase*

The heat balance for the gas phase is made on a single cell (channel) of the i th monolith ring, Fig. 4, since all cells within each ring are equivalent.

$$\frac{dT_{g_i}}{dz} = \alpha(T_{s_i} - T_{g_i}) \quad (8)$$

with

$$\alpha = \frac{2(l+d)}{ld} \frac{h}{\rho \langle v \rangle C_p} = \sigma St \quad (9)$$

where σ is the surface-to-volume ratio of the monolith cells and St is the Stanton number. In applying eq. (8), an assigned value of the solid temperature, T_{s_i} , is considered. At mid-distance, $\zeta = 0.5$, eq. (4) gives:

$$T_{s_i} = T_{g_i} + (T_{w_i} + T_{w_{i-1}}) \frac{\sinh(N/2)}{\sinh N} - T_{g_i} \frac{\tanh(N/2)}{\sinh(N/2)} \quad (10)$$

which for small N (≤ 0.5) reduces to the arithmetic mean,

$$T_{s_i} \approx \frac{T_{w_{i-1}} + T_{w_i}}{2}. \quad (11)$$

Since T_{w_i} as given by eq. (7) is a function of all the monolith cell gas temperatures, which are changing in the z -direction, the following system of n simultaneous differential equations must be solved,

$$\frac{dT_{g_i}}{dz} = f_i(T_w, T_{g_1}, T_{g_2}, \dots, T_{g_n}), \quad i = 1, 2, \dots, n \quad (12)$$

with prescribed initial conditions at the monolith inlet ($z = 0$), e.g. uniform inlet gas temperature, $T_{g_i} = T_{g_0}$ ($z = 0$), $i = 1, 2, \dots, n$. The system of linear differen-

tial eqs (12) with constant coefficients, is solved analytically to calculate the monolith gas temperatures, T_{g_i} , at any axial distance from the inlet. The monolith wall temperatures, T_{w_i} , are then calculated from eq. (7).

Parametric effects

The model predictions depend on the values of the parameters N and α defined in eqs (2) and (9), respectively. The parameter $N = \left(\frac{hl^2}{k_s w}\right)^{1/2}$ can be expressed as the square root of the ratio of (conduction resistance)/(convection resistance). Large values of N would reduce heat conduction through the solid resulting in lower bed temperatures. In the limit (as $N \rightarrow \infty$), $T_{w_0} = T_{g_i}$, eq. (7), $T_{s_i} = T_{g_i}$ ($i = 1, 2, \dots, n$), eq. (10). Hence, flat temperature profiles are calculated for large heat transfer coefficients, h , low solid thermal conductivity, k_s , or small monolith wall thickness, $2w$, all corresponding to large values of N . Conversely, small values of N , enhance heat conduction. In the limit (as $N \rightarrow 0$), $T_{w_0} \rightarrow T_w$, and all $T_{w_i} \rightarrow T_w$ [eq. (7)], i.e. "step-function" temperature profiles are obtained for all monolith wall temperatures. The cell size, l , only has a minor effect on the model. For a change in l (keeping σ constant), the product $nN = R(h/k_s w)^{1/2}$ is independent of l , and the model parameter $\alpha = \sigma St$ changes only slightly (through $\rho \langle v \rangle$, which depends on ε). The effect of the parameter α on the calculated gas temperatures is "step-function" axial profiles (from the initial gas temperature to T_w) for large values of α or flat temperature profiles for very small α . Large values of h or low mass flow velocities give large α . In solving the model equations, it was found that variation of α through the heat transfer coefficient alone has but a small overall effect on the calculated temperatures. This is because both parameters N and α change in the same direction as h changes, thus, offsetting the impact on the model. Of course, in the limit (for $h \rightarrow \infty$), the controlling model parameter is N (rather than α) and flat temperature profiles are obtained everywhere in the monolith.

MONOLITH MODEL COMPARISONS WITH EXPERIMENTS

In the following examples, the model developed in the previous section is used to calculate gas and solid

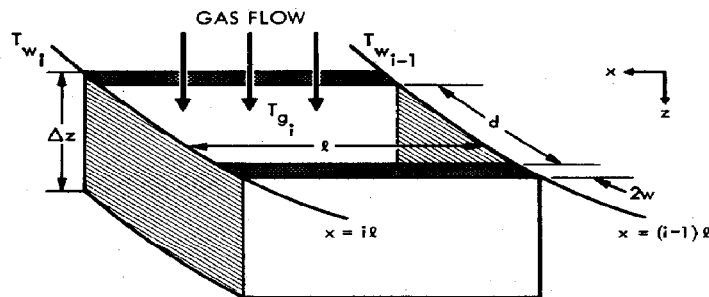


Fig. 4. Cell element within the i th monolith ring considered for the gas-phase heat balance.

wall temperatures within a cylindrical honeycomb monolith, 6.021 cm I.D. \times 7.6 cm length. The steady-state profiles are obtained for different flow rates of nitrogen at prescribed gas inlet temperatures and for a nitrogen external monolith wall temperature, T_w . Experimental comparisons are made using a metal monolith of Fecralloy[®] substrate made by Johnson Matthey, Inc. The geometric parameters and solid thermal conductivity of this monolith (Pratt and Cairns, 1977) are shown in Table 1.

The real monolith consists of sinusoidal cells while the simulated one has cells of rectangular cross-section, $A_c = ld$. The parameters of the simulated monolith were calculated here for a choice of $l = 0.1115$ cm, which gives an integer number of rings, $n = 27$. The wall thickness, $2w$, was kept the same as in the real monolith. The value of the cell cross-sectional area, A_c , was chosen equal to that in the real monolith. All other parameters were calculated based on the relations: $A_w = 2wl$, $n_c = 1/(A_c + A_w)$, $\varepsilon = n_c A_c$, $\sigma = 2(l + d)/ld$ and $G.S.A. = \sigma\varepsilon$. An account of all symbols is given in the Notation.

The gas properties (μ , k_g , C_p) were calculated at a constant average film temperature, T_f , estimated here for cells of a ring located halfway between the monolith wall and centreline, and assumed to be the same for all rings. The analytical solution for cylindrical tubes of constant wall temperature (Grigull and Tratz, 1965) was used to calculate Nusselt numbers, Nu . This gives Nu in terms of the Graetz number, $X^* = 4z/(D_H Re Pr)$, with Re and Pr the Reynolds and Prandtl numbers, respectively. The Reynolds number is expressed as: $Re = D_H \rho \langle v \rangle / \mu$, with $\rho \langle v \rangle$ the mass flux through each monolith cell, $\rho \langle v \rangle = 4G/(\pi D^2 \varepsilon)$. A constant value of 0.74 was used for the Prandtl number (Perry and Chilton, 1973). For high values of X^* , the asymptotic Nusselt numbers corresponding to fully-developed laminar flow are obtained. These are given in Table 2 for different channel geometry (Shah and London, 1971). In the examples considered below the Nusselt numbers were higher than these asymptotic values even close to the monolith exit ($z = 7.6$ cm).

In order to simplify the calculations, an average value of Nu was considered, uniform with z , from

Table 1. Parameter comparison in the real and simulated metal monoliths

Parameter	Fecralloy [®] monolith	Simulated monolith
Void fraction, ε	0.890	0.963
Geometric surface area, $G.S.A.$, cm^{-1}	32.30	32.23
Surface to volume ratio (cell), $\sigma = G.S.A./\varepsilon$, cm^{-1}	36.29	33.48
Hydraulic diameter (cell), D_H , cm	0.1102	0.1195
Cell area, A_c , cm^2	0.0144	0.0144
Cell density, n_c , cells/ cm^2	62	67
Wall thickness, $2w$, cm	0.005	0.005
Solid thermal conductivity, k_s , cal/cm/s/ $^\circ\text{C}$	0.06	0.06

Table 2. Asymptotic Nusselt numbers for laminar flow in ducts

Channel geometry	Nu_H^\dagger	Nu_T^\ddagger
Circular	4.364	3.655
Square	3.608	2.976
Triangular	3.111	2.470
Sinusoidal	2.617	2.120

[†]Constant wall heat flux.

[‡]Constant wall temperature.

which the heat transfer coefficient, $h = Nuk_g/D_H$, was calculated (the same for all cells, $h_i = h$, $i = 1, 2, \dots, n$). The error introduced by this assumption was estimated by also calculating heat transfer coefficients for fully-developed laminar flow using the asymptotic value of 2.976 for Nu (square-cell geometry, Table 2). The interesting finding was that the model predictions were rather insensitive to variations in the heat transfer coefficient. As discussed in the previous section, this is due to the effect of h on the model parameters N and α . For example, for a given cell size, l , which specifies n , a higher value of h would give higher N (and nN) that would reduce heat conduction through the solid, while α would also be higher tending to increase interphase heat transfer (from the solid to the gas phase). The overall effect on the calculated temperatures was found to be small. Hence, in the following examples, the assumption of fully-developed laminar flow throughout the monolith length is used to calculate h .

In order to check the model predictions with experiments the Fecralloy[®] monolith was heated in a flow of nitrogen under non-adiabatic conditions. The monolith was instrumented with 35 Inconel-sheathed, K-type thermocouples positioned inside cells at various bed locations and held in place by sealing the exit end of each cell. Each thermocouple junction was secured against the cell wall by a metal insert. The monolith wall (rather than gas) temperatures were, thus, measured by the inserted thermocouples. The monolith was tightly packed inside a thin-wall stainless steel tube. The reactor wall temperatures were controlled by external heating with a three-zone electric Mellen furnace. A schematic of the experimental system is shown in Fig. 5. Different, but constant, flow rates of nitrogen were measured with a mass flowmeter and passed downward through the reactor. The inlet gas temperatures were monitored by four K-type thermocouples inserted from the bottom and extending 1/16" from the top of the monolith segment.

Case 1

The steady-state heating of 5 lb/hr of nitrogen gas flowing through the metal monolith is considered in this case. The measured monolith wall temperature, T_w , was in the range of 954–1015 K, while the inlet gas temperature varied from 811 K at the centreline to 890 K close to the wall. The model equations were solved for $T_w = 994$ K and for a "step-function"-

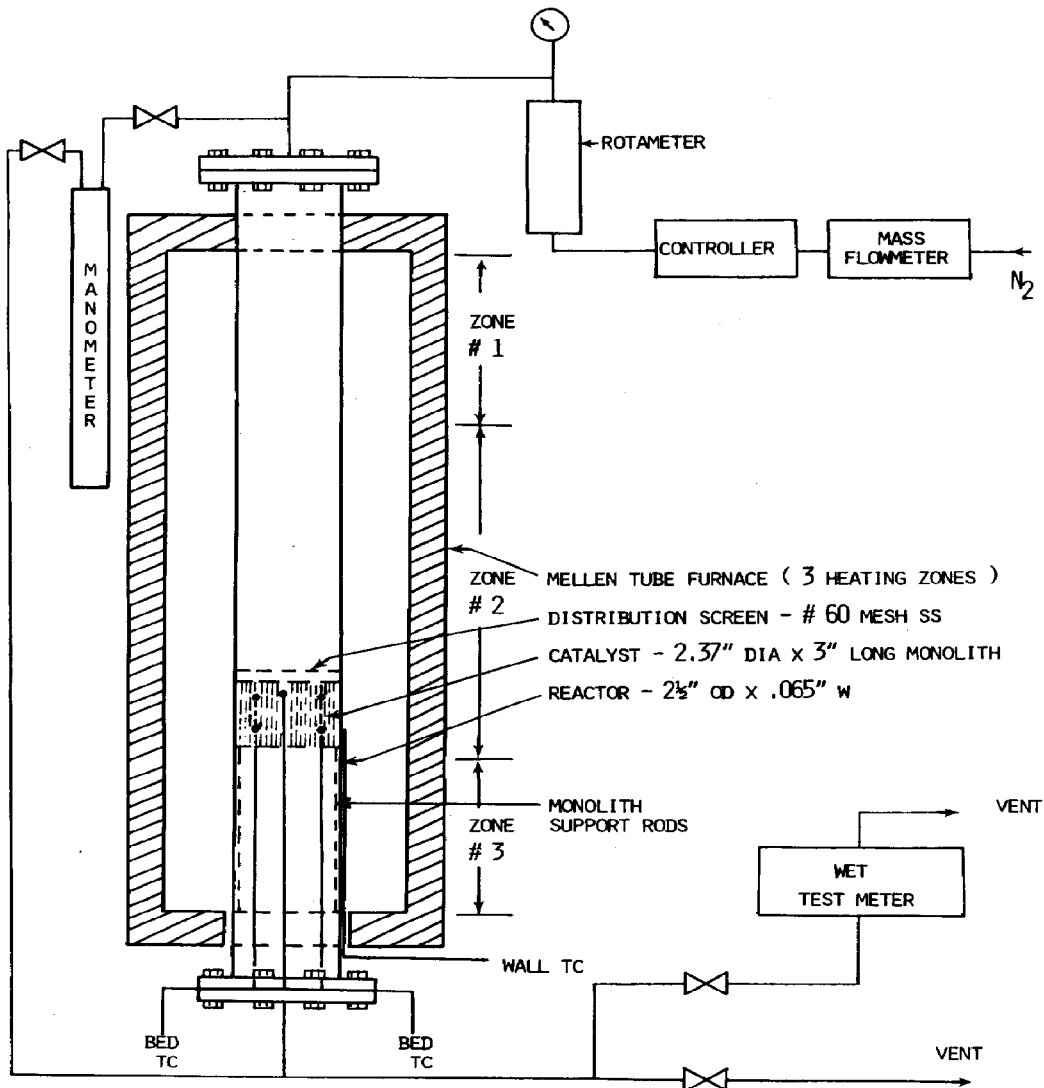


Fig. 5. Schematic of the experimental system.

inlet gas temperature: $T_{g_0} = 811 \text{ K}$, $0 \leq x < R/2$; $T_{g_0} = 853 \text{ K}$, $R/2 \leq x \leq R$. The gas properties were calculated at 853 K, and the corresponding heat transfer coefficient for fully-developed laminar flow ($Nu_T = 2.976$) was equal to $3.44 \times 10^{-3} \text{ cal/cm}^2/\text{s}/^\circ\text{C}$. The geometric parameters and solid thermal conductivity of the simulated monolith listed in Table 1 were used to calculate the model parameters N and α : $N = 0.534$ and $\alpha = 18.403 \text{ cm}^{-1}$. The assumption for T_s , [eq. (11)] is still valid for this value of N . Note that if N was ≥ 0.5 , a finer cell size, l , would be chosen to lower N to ≤ 0.5 . As discussed previously, this would have only a minor effect on the calculated temperatures.

Figure 6 shows calculated and experimental axial wall temperature profiles at reduced radial distances, $x/R = 0.0$ (centreline), 0.67 and 1.0 (wall). For the conditions of this example, over 70% of the tempera-

ture change has taken place by the end of the first half of the monolith length. The deviation of the calculated from the experimental curves of Fig. 6 is less than 10% at all radial distances, and for the total monolith length. Taking into account the simplified approach adopted in developing the model, these results are very encouraging. Moreover, no heat loss from the monolith was considered in the model. However, under "static" conditions (in "no-flow" experiments), the metal monolith was non-isothermal at steady-state, losing heat from the bottom. This can, in part, explain the lower values of the experimental temperatures of Fig. 6.

Case 2

The model predictions are compared here with experimental data for heating the monolith at a higher

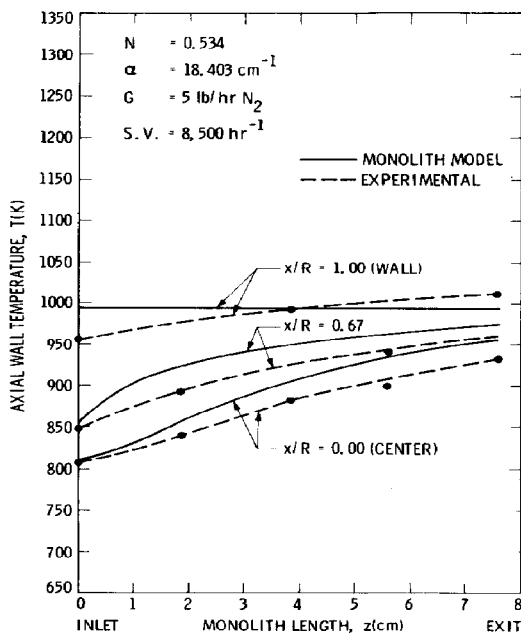


Fig. 6. Calculated and experimental axial wall temperature profiles in the Fecralloy metal monolith (Table 1) used for heating 5 lb/hr nitrogen. The model was solved for $T_w = 994$ K, and $T_{g_0} = 811$ K ($0 \leq x/R < 0.5$), $T_{g_0} = 853$ K ($0.5 \leq x/R \leq 1$).

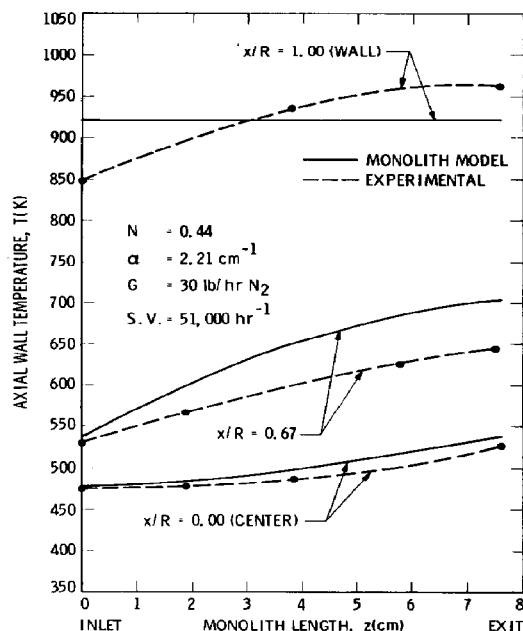


Fig. 7. Calculated and experimental axial wall temperature profiles in the Fecralloy metal monolith (Table 1) used for heating 30 lb/hr nitrogen. The model was solved for $T_w = 922$ K, and $T_{g_0} = 477.6$ K ($0 \leq x/R < 0.5$), $T_{g_0} = 533$ K ($0.5 \leq x/R \leq 1.0$).

flow rate of nitrogen, $G = 30$ lb/hr (corresponding to a space velocity of $\sim 51,000$ hr $^{-1}$). The model was used with monolith wall temperature equal to the average experimental value of 922 K, and inlet gas temperatures of 477.6 K in the range $0 \leq x < R/2$ and 533 K for $R/2 \leq x \leq R$. The calculated values of the parameters N and α in this case were: $N = 0.440$ and $\alpha = 2.21$ cm $^{-1}$. Figure 7 shows experimental and calculated axial wall temperature profiles at three reduced radial distances, $x/R = 0.0, 0.67$ and 1.0 . Similar observations as in Case 1 are made, the model deviation from experiment being $\sim 10\%$. Because of higher flow rate, the temperature profiles are much flatter in this case. In the model this is accounted for by the lower value of the parameter α , which is inversely proportional to $\rho \langle v \rangle$. It is noteworthy that higher flow rate conditions did not have a significant effect on the approach of the calculated to the experimental temperature profiles.

EXPERIMENTAL COMPARISONS WITH PACKED BEDS

The experimental system shown in Fig. 5 was also used to study the heating of a packed bed of alumina pellets at identical test conditions to those used for the metal monolith. The packed bed consisted of small ($1/8" \times 1/8"$) cylindrical pellets with $G.S.A. = 11$ cm 2 /cm 3 and void fraction (bed porosity) of 0.40. While this geometric surface area is only one third of the corresponding monolith value, selecting an even smaller size pellet bed (higher $G.S.A.$) may be impractical for most industrial applications because of

associated larger pressure drops. On the other hand, a larger size pellet bed, which conducts heat better (Smith, 1970) and causes lower pressure drop, would have too low an activity (because of very low $G.S.A.$) for meaningful comparisons with the monolith under actual reaction conditions.

Figure 8 shows axial bed temperature profiles obtained experimentally for this packed bed along with corresponding experimental profiles in the metal monolith shown before in Fig. 6 for a mass flow rate of nitrogen equal to 5 lb/hr (space velocity $\sim 8,500$ hr $^{-1}$). The centreline temperature is higher for the metal monolith throughout the bed length. Hence, the radial temperature difference between the centreline and reactor wall is lower in the monolith than in the pellet bed. This is particularly important immediately downstream of the reactor inlet where temperature gradients are largest under reaction conditions. Another desirable heat transfer feature of the monolithic geometry is displayed by flatter radial temperature profiles than in pellets. This is shown in Fig. 9 at different reduced axial bed lengths (z/H) for the same conditions as in Fig. 8.

For high space velocities or large temperature differences between the inlet gas stream and reactor wall, the differences in heat transfer properties between the monolith and packed bed geometries are magnified. An example is shown in Figs 10 and 11, which compare axial and radial temperature profiles, respectively, in the honeycomb metal monolith and the packed bed for a flow of 10 lb/hr nitrogen (S.V.

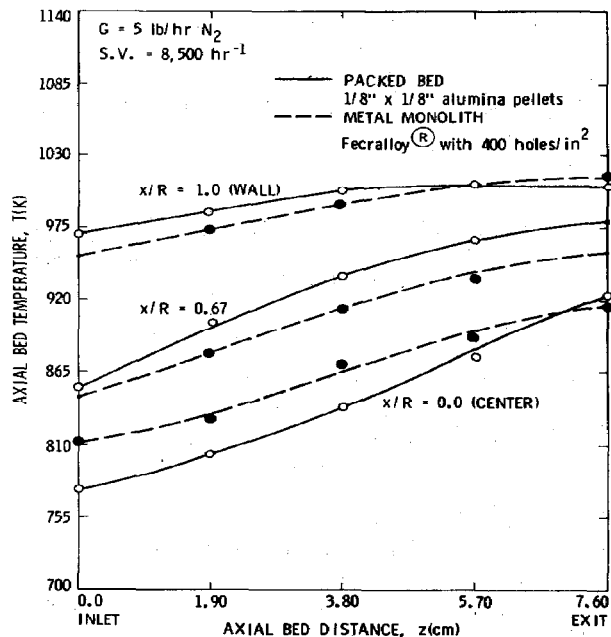


Fig. 8. Experimental axial temperature profiles in the Fecralloy metal monolith (Table 1) and a packed bed of alumina pellets ($1/8" \times 1/8"$ cylinders) used for heating 5 lb/hr nitrogen under similar inlet gas and external wall temperatures.

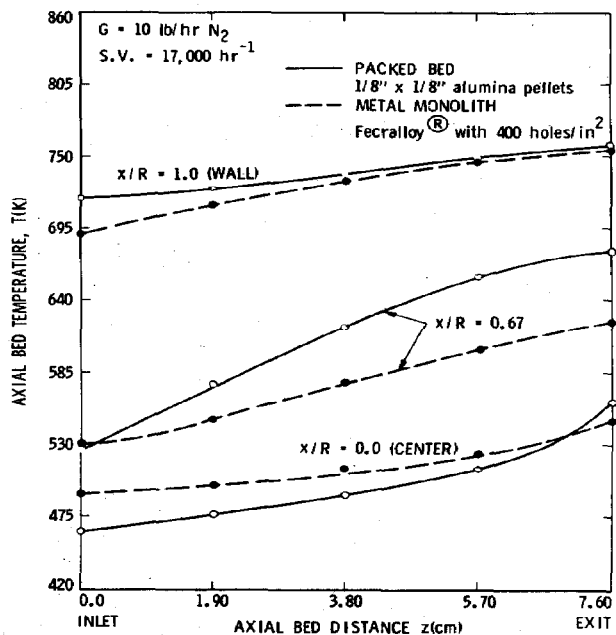


Fig. 10. Experimental axial temperature profiles in the Fecralloy metal monolith (Table 1) and a packed bed of alumina pellets ($1/8" \times 1/8"$ cylinders) used for heating 10 lb/hr nitrogen under similar inlet gas and external wall temperatures.

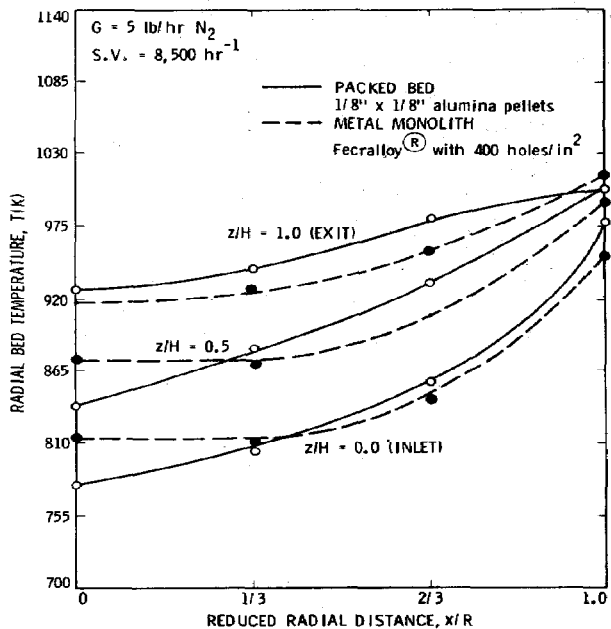


Fig. 9. Experimental radial temperature profiles in the metal monolith and pellet bed at the conditions of Fig. 8. z/H is a reduced axial distance with H denoting the total bed height.

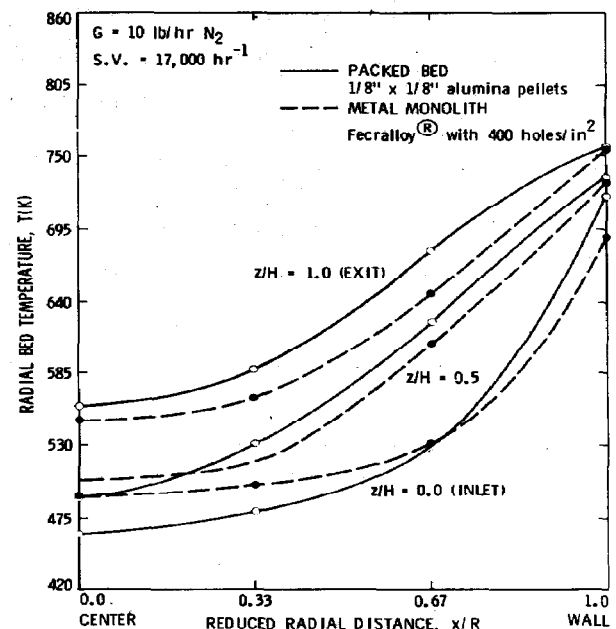


Fig. 11. Experimental radial temperature profiles in the metal monolith and packed bed at the conditions of Fig. 10.

$\sim 17,000 \text{ hr}^{-1}$) at approximately the same inlet gas and external wall temperatures. The monolith conducts heat better in the radial direction through its

continuous solid matrix. This is reflected by higher temperatures at (and close to) the bed centreline. However, the packed bed is superior near the reactor

wall due to cross flow of gas (enhanced radial heat convection and turbulent diffusion). At long bed lengths (specified by the operating conditions) the pellets conduct heat better than the honeycomb monolith everywhere in the bed.

SUMMARY AND CONCLUSIONS

A simple model has been developed to treat the heat transfer problem in non-adiabatic honeycomb monoliths. A real monolith was simulated by the two-phase structure shown in Fig. 2, and steady-state heat balances were written separately for the solid and gas phases of the simulated monolith. In the absence of chemical reaction, the model was solved analytically to give solid and gas temperature profiles radially and axially within the monolith reactor.

The assumptions used in developing the model appear adequate for this first generation approach. Heat transfer in the honeycomb monolith is enhanced at low values of the parameter N (i.e. low h , l or large k_s , w) and large values of α (i.e. large h , σ or low $\rho \langle v \rangle$). In solving the model, it was found that the assumption of uniform heat transfer coefficient, h , in all the monolith channels is good, since the calculated temperatures were rather insensitive to changes in h (compensating effect on the parameters N and α). The choice of cell size, l , for constant σ , does not significantly affect the model predictions. For eq. (11), however, to be valid (low N), a fine cell increment is chosen. In general, it was found that for all flow rates (space velocities) the calculated temperatures were typically within 10% of the experimental values which is rather good considering the assumptions of the model. The approach presented here may, thus, be used as a simple computational technique for expeditious comparisons with experimental data. By including reaction terms in the model, heat and mass transfer in a non-adiabatic monolith may be calculated numerically by a variation of the present model.

Experimental heat transfer comparisons of a Fecralloy® metal monolith with a packed bed of alumina pellets have revealed the conductive heat transfer merits of honeycomb monoliths in the top part of the reactor and around the bed centreline. The convective element of heat transfer, characteristic of packed beds, was significant in the vicinity of the reactor wall. The significance of these findings is two-fold. First, it appears that honeycomb metal monoliths may be used to retrofit existing reactors (or heat exchangers) by replacing a certain length of pellets at the most energy-demanding location (e.g. inlet part) of the bed. This will result in higher energy efficiency because of reduced external heat requirements. Secondly and, perhaps, more importantly the data presented here has indicated certain directions to be taken for catalyst design improvement and optimization. For example, a novel monolith geometry allowing for radial gas mixing may combine the best heat transfer features of both the honeycomb monolith and the pellet bed geometries and result in still higher savings in an industrial application. Experimental

work with corrugated metal strips (Flytzani-Stephanopoulos and Voecks, 1986), currently in progress in this lab has shown considerable heat transfer improvements over packed beds under a variety of operating conditions.

Acknowledgement—This work was supported by the Phosphoric Acid Fuel Cell Program managed by NASA Lewis Research Center for DOE, under Interagency Agreement No. DE-AI01-80-ET17088.

NOTATION

A_c	cell cross-section, ld , cm ²
A_w	solid wall area per cell, $2wl$, cm ²
C_p	heat capacity of the gas, cal/g/°C
d	cell width, cm
D	monolith diameter, cm
D_H	hydraulic diameter (cell), $4/\sigma$, cm
G	mass flow rate, lb/hr
$G.S.A.$	geometric surface area (surface-to-volume ratio), monolith, $\sigma\epsilon$, cm ² /cm ³
h	heat transfer coefficient, cal/cm ² /s/°C
H	axial monolith length, cm
i	location of monolith ring, $i = 1, \dots, n$
k_g	gas thermal conductivity, cal/cm/s/°C
k_s	solid thermal conductivity, cal/cm/s/°C
l	radial cell length, cm
n	total number of monolith rings, R/l
n_c	monolith cell density, $1/(A_c + A_w)$, holes/cm ²
N	monolith model parameter, $(hl^2/k_s w)^{1/2}$
Pr	Prandtl number, $C_p \mu/k_g$
R	monolith bed radius, cm
Re_c	Reynolds number, $D_H \rho \langle v \rangle / \mu$ (monolith cell)
St	Stanton number, $h/(\rho \langle v \rangle C_p)$
T_f	average film temperature, gas phase, K
T_{g_0}	inlet gas temperature, K
T_{g_i}	gas temperature, i th monolith ring, K
T_{s_i}	solid temperature, i th monolith ring, K
T_{w_i}	solid wall temperature, i th monolith ring, K
T_w	external monolith wall temperature, K
$\langle v \rangle$	average fluid velocity in monolith cells, $4G/(\rho \pi D^2 \epsilon)$, cm/s
w	half wall thickness, monolith, cm
x	radial distance, cm
X^*	Graetz number, monolith cells, $4z/(D_H Re Pr)$
z	axial distance, cm

Greek letters

α	monolith model parameter, σSt , cm ⁻¹
β_i	wall temperature gradient, i th monolith ring
ϵ	percentage open frontal area, monolith, $n_c A_c$
μ	fluid viscosity, g/cm/s
ξ	dimensionless radial distance, $(x - (i - 1)l)/l$
ρ	fluid density, g/cm ³
σ	surface-to-volume ratio, monolith cell,

$$\frac{2(l+d)}{ld} = 4/D_H = G.S.A./\epsilon, \text{ cm}^{-1}$$

REFERENCES

- Aris, R., 1977, *Physicochemical Hydrodynamics Series 2*. Advance Publications, London.
- Bird, R. B., Stewart, W. E. and Lightfoot, E. N., 1960, *Transport Phenomena*, pp. 288–290. Wiley, New York.
- Flytzani-Stephanopoulos, M. and Voecks, G. E., 1981, Conversion of hydrocarbons for fuel cell applications. Final Report to DOE, DOE/ET-11326, Jet Propulsion Laboratory Publ. 82-37, Pasadena, California.
- Flytzani-Stephanopoulos, M. and Voecks, G. E., 1986, Enhanced heat-transfer catalyst supports. *Chem. Engng Sci.* to be submitted.
- Grigull, V. and Tratz, H., 1965, Thermischer Einlauf in ausgebildeter laminarer Rohrströmung. *Int. J. Heat Mass Transfer* **8**, 669.
- Heck, R. H., Wei, J. and Katzer, J. R., 1976, Mathematical modeling of monolithic catalysts. *A.I.Ch.E. J.* **22**, 477–484.
- Hegedus, L. L., 1975, Temperature excursions in catalytic monoliths. *A.I.Ch.E. J.* **21**, 849–853.
- Perry, R. H. and Chilton, C. H., 1973, *Chemical Engineer's Handbook*, 5th edn, pp. 3–239. McGraw-Hill, New York.
- Pratt, A. S. and Cairns, J. A., 1977, Noble metal catalysts on metallic substrates. *Platinum Metals Rev.* **20**, 74–83.
- Shah, R. K. and London, A. L., 1971, Laminar flow forced convection heat transfer and flow friction in straight and curved ducts—a summary of analytical solutions. Tech. Report No. 75, Stanford University, Palo Alto, California.
- Smith, J. M., 1970, *Chemical Engineering and Kinetics*, 2nd edn. McGraw-Hill, New York.
- Votruba, J., Sinkule, J., Hlavacek, V. and Skrivanek, J., 1975, Heat and mass transfer in monolithic honeycomb catalysts—I. *Chem. Engng Sci.* **30**, 117–123.